

Experimental and numerical simulation of a novel magnetic pole repulsive passive damper for vibration control

Saran Sathish Kumar¹, Amudhan Vijayakumar¹, Daniel Cruze¹ and Hemnath Kasaram¹

¹ Hindustan Institute of Technology and Science, Department of Civil Engineering, Chennai, Tamil Nadu, India

Corresponding author:

Daniel Cruze
danielckarunya@gmail.com

Received:
May 18, 2023

Accepted:
August 21, 2023

Published:
October 27, 2023

Citation:

Satish Kumar, S.; Vijayakumar, A.; Cruze, D.; and Kasaram, H. (2023). Experimental and numerical simulation of a novel magnetic pole repulsive passive damper for vibration control. *Advances in Civil and Architectural Engineering*. Vol. 14, Issue No. 27. pp.114-130
<https://doi.org/10.13167/2023.27.8>

ADVANCES IN CIVIL AND ARCHITECTURAL ENGINEERING (ISSN 2975-3848)

Faculty of Civil Engineering and Architecture
Osijek
Josip Juraj Strossmayer University of Osijek
Vladimira Preloga 3
31000 Osijek
CROATIA



Abstract:

This article presents a novel magnetic pole repulsive damper (MPRD) incorporating neodymium magnetic repulsive blocks and springs. The study explores the mechanical properties of the springs and magnetic blocks through numerical simulations using ANSYS and experimental evaluation. To gain deeper insights into the behaviour of the MPRD, an accurate and high-fidelity finite element model was developed. The evaluation process involved a comprehensive comparison between the numerical simulations and experimental tests, explicitly focusing on cyclic compression–tension forces. The study encompassed the functioning, design implications, fabrication technique, mechanical performance, and numerical simulation for the cyclic compression–tension forces of the MPRD. The cyclic compression–tension tests revealed a gradual increase in force, with the MPRD achieving an ultimate force of 2,877 kN. The MPRD exhibited robust hysteresis behaviour in cyclic loading, showing its capacity to undergo and uphold the stability of the combination of its materials. The cyclic compression–tension results indicated the maximum force carrying capability of the damper. This resilience implies its full reusability in such scenarios. The comparison between cyclic compression–tension tests confirmed the alignment between the numerical simulation and experimental investigation.

Keywords:

magnetic pole repulsive damper (MPRD); passive damper; cyclic behaviour; displacement control test

1 Introduction

The extent of damage has increased with the size and frequency of earthquakes in recent years. In addition to causing secondary damage, including human casualties and facility maintenance expenses, earthquakes can damage and even result in collapse of a variety of structures. Therefore, it is essential to create equipment with superior seismic activity and semi-permanent qualities to limit and stop earthquake damage. Owing to their weight, structures are often built to withstand vertical loads; nevertheless, limiting the lateral stresses caused by seismic motion is necessary to reduce earthquake damage. Control of the structure, which can be active, semi-active, or passive, is used in various ways to decrease vibration and regulate the displacement of a structure during seismic events [1]. Using sensors, controllers, and actuators, active control systems can boost structural damping without compromising rigidity. The sensors track the system response variables, while the controller interprets the data and delivers control signals to the actuators. These signals cause the actuators to create forces that may differ from the controller's instructions. Real-time operation requires electricity. Decentralised and self-regulating PID controller-based mechanisms using magnetorheological dampers are utilised for earthquake protection of tall building structures. Numerical simulations showed that the combined approach produced superior earthquake-tracking precision of 95,54 % and 99,27 % with and without faults, respectively, compared with other control mechanisms, demonstrating its potential for real-world applications [2]. Passive structural control depends on the equipment and materials used to make the damper and is not affected by the forces generated by an earthquake or wind. The primary objective of passive control systems is to minimise the contribution of major structural components to the plastic-deformation-based dissipation of input energy [3]. Passive control systems include base isolators, metallic yielding dampers, friction dampers, viscous and viscoelastic dampers, tuned mass dampers, and liquid dampers [4-7]. Li developed an innovative shape-memory alloy damper to reduce earthquake responses. Cyclic tests and nonlinear time-history analysis showed that the damper with deformation amplification exhibited superior seismic performance, with peak displacement, inter-storey drift, acceleration and residual displacement reduction ratios of up to 27,32 %, 39,73 %, and 95,33 %, respectively, during strong earthquakes. A deformation amplification coefficient range of 2,0-3,0 was suggested [8]. Dong et al. conducted an experimental investigation in which nonlinear viscous dampers were used to simulate the effects of a design basis earthquake (DBE) and the maximum considered earthquake (MCE) on a three-storey structure. The building had a moment-resisting frame with small beam sections, and the results demonstrated excellent seismic activity, even for a structure built to only 60% of the necessary base shear strength. This simplified design procedure can achieve the performance objectives with lower base shear design strength than conventional MRFs [9-11]. Through testing and research, the performance and constraints of the steel dampers were revealed by their yield and mechanism, making them the most representative of all the present dampers [12-16]. Unlike active dampers, passive dampers, such as viscoelastic dampers [17], do not require sensors or external energy sources. A damper in structural components reduces seismic activity by producing a shear force, and its performance has been demonstrated through numerical simulations and experiments [18-20]. Consequently, much research has been conducted recently on a technology that simplifies the repair of damaged damper components or on a smart technology that can employ new materials to mitigate the permanent deformation of dampers. An innovative damper was built based on a novel idea using modern materials with recentring properties [21]. These dampers have been analysed in high-rise building structures and have reduced the seismic force of natural disasters [22, 23]. Analysis and performance evaluation of a damper with a high damping force using the contact force of permanent magnets was performed [24-28]. In recent years, computational methods such as the finite element approach have been used to improve the damper structure [27-31]. However, permanent deformation occurs when the general damper device reaches the permitted capacity of the seismic force, leading to inter-floor displacement and long-term displacement

of the building [28]. In addition, different spring materials have been analysed in Ansys [30-33].

Consequently, the device acts as a smart damper. The most sophisticated friction damper offers adaptive control of buildings against earthquakes and is known as the variable friction damper. The varying friction is managed using a piezoelectric actuator [34, 35]. In steel frames with chevron bracing, the design relationships for two types of yielding elliptical dampers were demonstrated to prevent brace buckling and improve energy dissipation. Two steel dampers with shear diaphragms were proposed in this study. It was discovered that the design relationships were suitable, with the diaphragms providing increased cyclic performance [36-38].

In this research, a comparison of the numerical simulation using ANSYS and the experimental performance of springs, magnets, and the proposed magnetic pole repulsive damper (MPRD) was carried out with the aim of increasing the seismic stability with a decrease in permanent deformation under the maximum force. The MPRD displays the force performance by employing springs and magnets. The elastic force of the spring is smart because it can support the force while being compressed and stretched, and automatically returns to its original state. In addition, as shown in earlier research, magnetic blocks have been employed to improve the energy dissipation capability, which is more vital than springs for withstanding forces. In addition, the springs can be compressed and tensioned to increase recentring, thereby reducing the residual displacement of the damper. The performance of the MPRD was assessed based on literature research and tests to identify material features, and it was found to be satisfactory. In this study, numerical analyses and experiments were conducted on the compression–tension behaviour of MPRDs.

2 Details of the proposed damper

The MPRD is a novel device designed to minimise the damage and residual displacement in buildings during earthquakes. This is achieved by effectively absorbing and dissipating the energy generated by seismic forces. The MPRD incorporates components such as neodymium magnets, a piston with a magnetic clamp, a magnetic clamp, and springs. These components work together to provide a mechanism for absorbing and controlling seismic forces in the tension and compression directions. By utilising the magnetic repulsive force along with the spring action, the MPRD aims to improve the seismic stability of joints of structures and reduce the risk of failure due to structural damage. Dampers are particularly useful in regions with seismic activity because they can significantly improve the resilience and robustness of structures, allowing them to survive strong earthquakes and reduce the risk of failure. Furthermore, using dampers in buildings improves the strength of the structure compared to standard techniques that depend primarily on component stiffening. Table 1 lists the results of the dimensional study of the proposed damper.

Table 1. Details of the proposed magnetic pole repulsive damper (MPRD)

Parameters	Dimensions
Length of the damper	1145 mm
Size of the damper	(1145 x 105 x 75) mm
Length of the piston with magnetic clamp	820 mm
Diameter of the piston	20 mm
Number of magnets	4 Nos
Size of magnets	(75 x 50 x 62,5) mm

3 Material testing

3.1 Experimental and numerical behaviour of the spring

A spring is an elastic machine component that, in response to any stress, deflects and, depending on the magnitude of the applied force, returns to its original form [30-33]. Springs

have many significant uses, owing to their capacities as vibration absorbers, as well as their capability to store potential energy via the deflection that occurs in response to the application of a force.

3.1.1 Simulation of the spring

A circular cross-sectional model of the utilised spring was developed using the ANSYS software, as shown in Figure 1a. The spring dimensions and specifications are listed in Table 2. Supports were applied at the ends of the spring to allow force to be applied at its centre. Static analysis of the spring was conducted using the Ansys Workbench with the Static structural module. The material selected for the spring was carbon steel (CS 80), and its properties, such as Poisson's ratio (0,3) and modulus of stiffness ($G = 200000$ MPa), are listed in Table 3. The spring was meshed with an element size of 8 mm for the analysis, as shown in Figure 1b. Spring connections were bonded on both sides using supports, with one support fixed to the ground and the other applying displacements for compression and tension separately, as tabulated in Table 4. The force reaction was then estimated to observe the force pattern, as shown in Figures 1c and 1d. With this numerical simulation, the spring behaviour under various loading conditions (5, 10, 15, 20, and 25 mm) was analysed, providing insights into its performance and response.

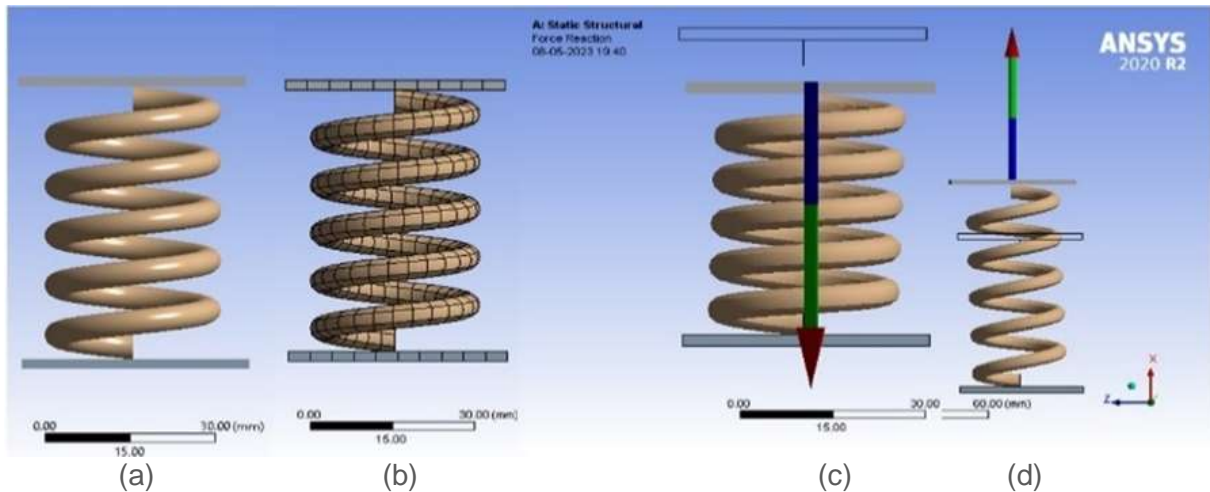


Figure 1. Schematic representation of the springs: a) geometry view, b) meshing of the spring, c) compression of the spring, d) tension of the spring

Table 2. Specification of the spring

Parameters	Dimensions
Length of the spring	50,0 mm
Mean radius of the spring (r)	26,0 mm
Diameter of the wire (d)	5,0 mm
Inner diameter	23,5 mm
Outer diameter	28,5 mm
Number of coils (n)	4 Nos
Deflection (δ)	25,0 mm

Table 3. Material properties of spring

Materials	Properties
Grade of the steel	CS 80
Elastic modulus	200000 MPa
Poisson ratio	0,3
Tensile strength	1397 MPa

3.1.2 Experimental setup of the spring

After the simulation, the prototype springs were tested using a tensile testing machine (TTM). Figure 2 shows the experimental arrangement of the springs in the machine, with the springs fixed on both sides. The force and deflection measurements were captured using a data collection system. The experiment was conducted under loading control with a gradual load application. The deflection of the springs was monitored at intervals of 5 mm as the force was applied up to a total deflection of 25 mm. This experimental setup allowed the characterisation of spring behaviour under different forces and provided data for comparison and validation with the simulation results.



Figure 2. Testing of the spring in the tensile testing machine

3.1.3 Behaviour of springs

The behaviour of the spring was analysed through numerical simulations using ANSYS and experimental testing using the TTM. Testing was performed under compression and tension with the force gradually increasing, and the deflection was monitored. In the compression tests, the maximum forces were 2,196 and 2, 2028 kN in the experiments and numerical simulations, respectively. Similarly, in the tension tests, the maximum forces were -1,972 kN in the experiments and -1,962 kN in the numerical simulations. The stiffness of the open coil spring in the experimental and numerical study was 0,0001 kN/mm. The comparison results showed that the variation around both the experimental and numerical simulation was 0,3% under compression and 0,5 % under tension, indicating good validation. The force versus deflection comparison results for compression and tension are shown in Figure 3, and the numerically simulated and experimental results are listed in Table 4. The agreement between the experimental and numerical results suggests the accuracy and reliability of the simulation in predicting spring behaviour.

Table 4. Comparison of the numerical and experimental results of the spring

Displacement (mm)	Simulation results		Experimental results	
	Maximum force in compression (kN)	Maximum force in tension (kN)	Maximum force in compression (kN)	Maximum force in tension (kN)
0	0	0	0	0
5	0,4000	-0,345	0,426	-0,345
10	0,8000	-0,690	0,712	-0,673
15	1,2050	-1,035	1,178	-1,145
20	1,7030	-1,512	1,625	-1,585
25	2,2028	-1,962	2,196	-1,972

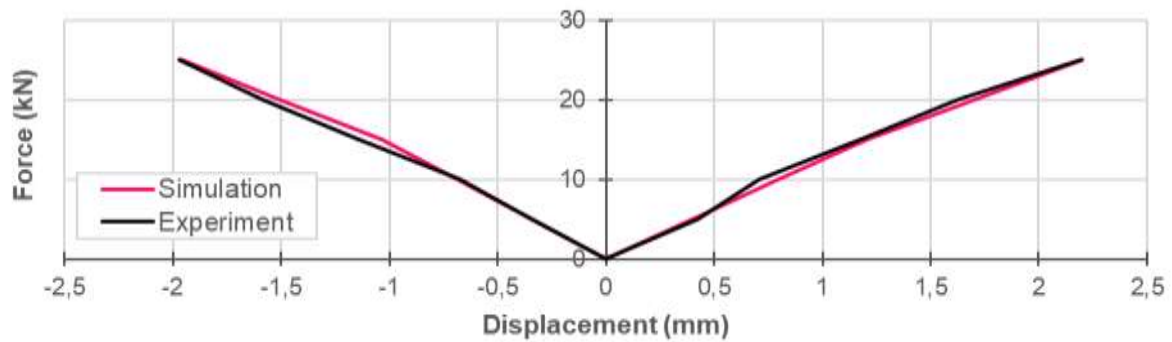


Figure 3. Comparison of the experimental and simulation results of the spring

3.2 Study on behaviour of the magnets

Magnets possess distinct polar directions, where the North Pole (N) attracts the South Pole (S), and the N–N and S–S poles repel each other. Various types of magnets, such as ferrite, neodymium, and samarium cobalt, are available. In this study, neodymium magnets were adopted based on the research conducted by Choi [33].

Neodymium and black ferrite magnets have been tested experimentally, and the results show that neodymium magnets offer a higher magnetic flux density than black ferrite magnets and are suitable for the intended application. The specifications of the magnet are listed in Table 5.

Table 5. Specifications of the magnet

Parameters	Details
Type of magnet	Neodymium magnets (NeFeb)
Grade of the magnets	N45
Number of magnets	4 Nos
Combined length of the magnets	75,0 mm
Combined breadth of the magnets	50,0 mm
Combined depth of the magnets	62,5 mm

3.2.1 Numerical study of the magnets

In the MPRD, magnets are crucial in generating the magnetic repulsive force. For effective functioning, the magnets must be aligned in a specific direction, such as in the SNSN–NSNS configuration shown in Figure 4a. The magnetic lines of force must be parallel to this direction to ensure the desired repulsive action.

A neodymium (N45) grade magnet was used in this study. The ANSYS software was employed to model the magnets, and Figure 4b shows a meshed magnet structure with a size of 3 mm. The neodymium magnets exhibited the expected behaviour, as depicted in Figure 4c, which presents the results obtained from the used magnets. The magnets were contained in an enclosure and surrounded by air to allow for a repulsive force. The enclosure was meshed to 3 mm. The direction of the magnets for the repulsive force was set by the material polarisation. The magnetic flux density of the neodymium magnets is approximately 1,32T. By observing and analysing the repulsive force of the magnets, it is possible to assess the performance and effectiveness of the magnet configuration in generating the desired repulsive action.

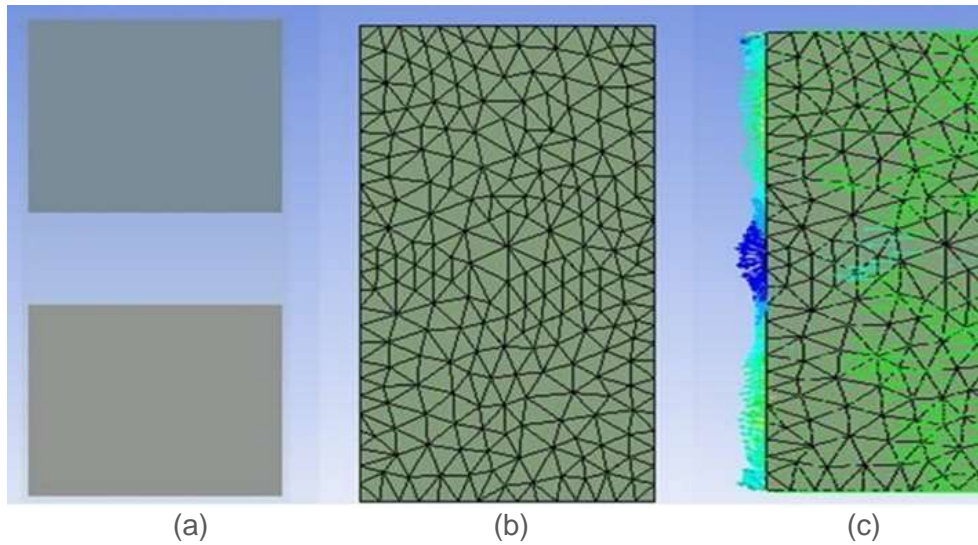


Figure 4. Schematic representation of the magnets: a) geometry view, b) structure of the magnets, c) obtained results

3.2.2 Experimental study of the magnets

To validate the numerical simulation results, the magnets were subjected to experimental testing using a TTM. The experimental setups for the ferrite and neodymium magnets are shown in Figures 5a and 5b, respectively. The boundaries of the magnets were fixed on both sides during testing.



Figure 5. Experimental set up of magnets: a) black ferrite magnet, b) neodymium magnet

3.2.3 Behaviour of magnets

Force control was employed, and displacement was measured at intervals of 5 mm. A comparison of the results of neodymium magnets with those of black ferrite magnets showed that the former outperformed the latter. The comparison results of the neodymium and black ferrite magnets are displayed in Table 6. Neodymium magnets are expected to exhibit properties that are superior to those of black ferrite magnets. This comparison helps understand and assess the performance and suitability of different magnets for MPRD applications. The experimental testing provided empirical evidence to support the numerical simulation results and aided in optimising the magnet selection for the MPRD design.

The behaviour of the repulsive magnetic force in the MPRD was studied through numerical simulations and testing using a TTM. The force was observed for every 5 mm in displacement, allowing for a comprehensive understanding of the performance of the magnet. The maximum force-carrying capacity of the magnets was determined to be 1,3894 kN in the experimental tests and 1,465 kN in the numerical simulation at a displacement of 5 mm. The variation between the experimental and simulated results is 7,69 %. These results are shown graphically in Figure 6, which visually represents the comparison results. The force versus deflection results for the magnets is tabulated in Table 7, which provides a comprehensive reference for their performance characteristics. This analysis and experimental testing provided valuable insights into the behaviour of the repulsive force of the magnet within the MPRD system.

Table 6. Comparison of the black ferrite magnet and neodymium magnets

Displacement (mm)	Black ferrite magnets (kN)	Neodymium (kN)
5	0,812	1,3894
10	0,662	1,1400
15	0,429	0,9340
20	0,239	0,7790
25	0,147	0,7000

Table 7. Force versus deflection for the magnets

Displacement (mm)	Simulation (kN)	Experimental (kN)
5	1,465	1,3894
10	1,149	1,1400
15	0,934	0,9340
20	0,774	0,7790
25	0,650	0,7000

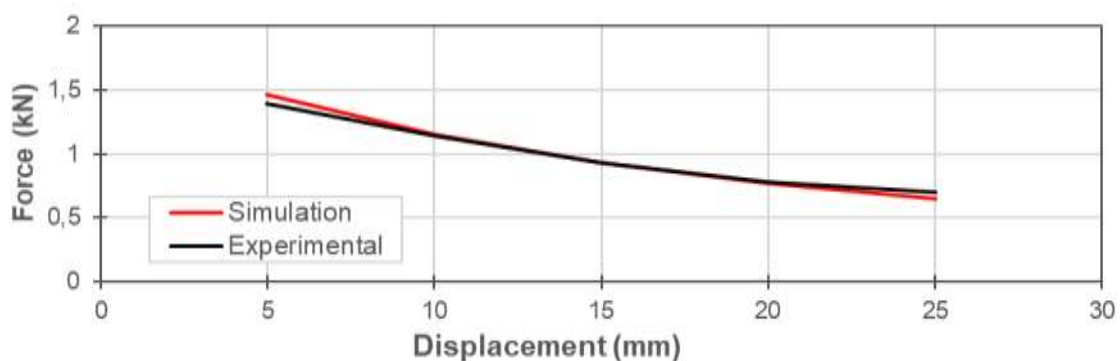


Figure 6. Compared experimental and simulation results of the magnet

4 Study on behaviour of the proposed damper

4.1 Modelling specification of the proposed damper (MPRD)

The MPRD is an interesting area of research that utilises repulsive magnetic forces and the compression and tension of springs to control the cyclic forces. Figure 7 shows the assembly of the 3D MPRD model. The damper was modelled as a combination of various small parts, as shown in Figure 8. The boundary conditions of the damper involved magnet clamps bonded to both sides of the springs, whereas the other sides of the springs were bonded to the damper body. When a force is applied, a spring is triggered, and magnetic repulsion controls the force, enabling the damper to withstand the forces and reduce the vibrations at the bottom. The dimensions of the MPRD specified in Table 8 were used for construction.

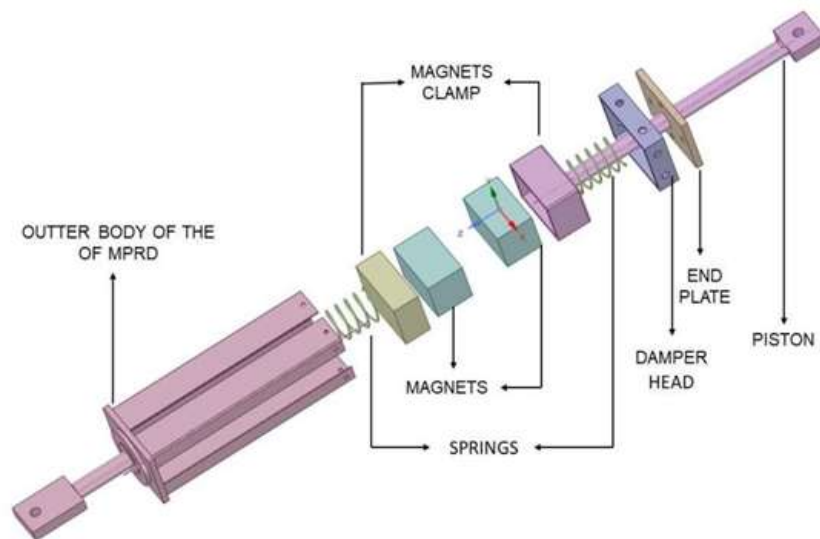


Figure 7. Assembly of parts of the MPRD

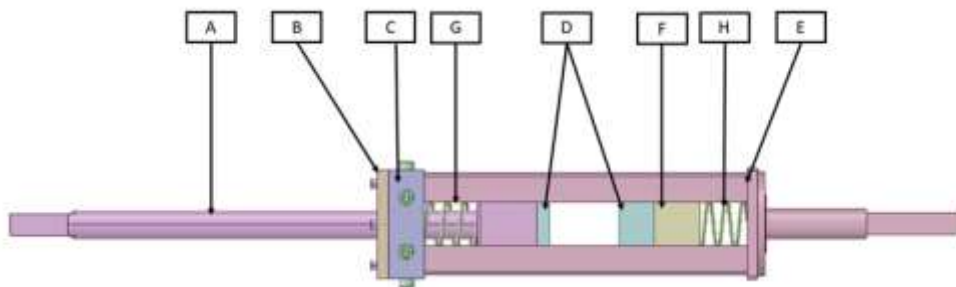


Figure 8. Schematic representation of the MPRD

Table 8. Dimensions of the MPRD

Parts	Length (mm)	Breadth (mm)	Depth (mm)	
A	Piston with magnet clamp	820,0	Φ 20,0	-
B	End plate	8,0	105,0	75
C	Damper head	25,0	105,0	75
D	Magnets	62,5	75,0	50
E	Damper body	26,0	92,0	66
F	Magnet clamp	46,0	75,0	50
G & H	Springs	50,0	28,5	5
-	Overall size of the damper	1145,0	105,0	75

4.2 Working mechanism of the proposed magnetic pole repulsive damper

The MPRD was specifically designed to withstand the seismic strains experienced by buildings. It utilises the motion of the piston and the action of springs to deliver its performance during sudden seismic stress. Springs play a crucial role in tension and compression to endure the applied force and return to their original shape. When the spring tension reaches a specific point, a repulsive magnetic action occurs. This allowed the springs to bear the maximum force capacity while maintaining their composition. Furthermore, as the compressive force increases, the bottom spring is activated, enabling it to compress and regain its shape owing to the inherent elasticity and stiffness of the spring. This combined mechanism ensures that the MPRD can effectively handle seismic forces and maintain its structural integrity.

4.3 Numerical simulation of the magnetic pole repulsive damper

4.3.1 Modelling of the damper

Researchers have used the finite-element method (FEM) to model dampers from various perspectives. The FEM technique separates the system geometry into small pieces and applies boundary conditions regarding forces and limitations to analyse unknown field variables such as displacement, strain, and stresses. In this study, the MPRD was examined using the well-known FEM program ANSYS. In the Space Claim, a 3D model of the MPRD was developed with thorough specifications prior to fabrication. The MPRD was then generated as a 3D model in Space Claim as part of the ANSYS Workbench. The material properties of the used steel, which has a density of $76,98 \text{ kN/m}^3$, are as follows: tensile yield strength of $0,25 \text{ kN/mm}^2$, compressive yield strength of $0,25 \text{ kN/mm}^2$, and tensile ultimate strength of $0,46 \text{ kN/mm}^2$. In the MPRD analysis, the springs were bonded to one side of the lower plate, and the bottom magnet clamp was also bonded. Another spring was located around the piston, with one side bonded to the top end-plate and the other side bonded to the top of the clamp, respectively. The magnets were bonded to the lower and upper clamps, and the boundary condition for the clamps was a frictional connection with the damper body. A magnetostatic numerical simulation of the MPRD was performed using the ANSYS platform following a series of steps to ensure accurate analysis and performance evaluation. A schematic representation of the MPRD was created using ANSYS software, as shown in Figure 9a. The MPRD was meshed with an element size of 8 mm to generate a finite element model, as shown in Figure 9b. The reaction force was estimated to observe the force pattern, as shown in Figure 9c.

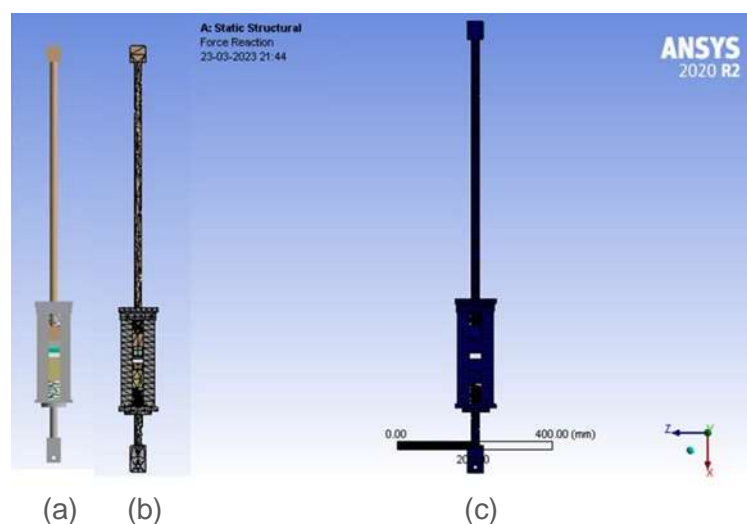


Figure 9. Schematic representation of the MPRD: a) geometry view, b) structure of the MPRD, c) numerical simulation of the MPRD

4.3.2 Cyclic compression–tension test

The primary purpose of this damper is to withstand seismic forces. As previously described, a cyclic loading pattern was used in this study. In addition to the magnetic repulsive force, the spring exhibited a loading pattern. Displacement was applied, and the force carried by the MPRD was monitored. The bottom of the MPRD was fixed to the ground. The magnets were arranged in an SNSN–NSNS formation, which caused the repulsive force to be activated. To observe the hysteresis behaviour of the MPRD, a deflection was applied at the top of the piston using the combined interaction model, and the force was observed. The MPRD was tested separately using displacement control at rates of 5, 10, 15, 20, and 25 mm/min for the vertical in-plane displacements applied from the top of the MPRD.

4.4 Experimental study on the proposed damper

4.4.1 Fabrication of the proposed damper

The passive MPRD operates using frictional constraints between the piston, magnetic clamp, and damper. When a force is applied in the positive direction, the repulsive force between the magnets generates a compressive force, and the effective springs are placed to encounter a direct force on the damper.

This design prevents damage to the damper body by placing springs between the lower clamp and damper body.

The springs stabilise the damper action, ensuring that the force is absorbed without harming the damper body. Conversely, when a force acts in the negative direction, the compression of the springs between the piston and damper reduces the force.

This mechanism allows the damper to effectively manage and control the forces in the compression and tension directions. The overall weight of the MPRD prototype was 9,544 kg (the weight of the piston with end plate, damper cap, spring, and magnet clamps is 3,28 kg; the weight of the damper body is 3,26 kg; the weight of the magnets is 2,26 kg; the lower magnet clamp is 0,39 kg, and the spring is 0,029 kg) and had a fully compressed length of 70 mm.

The total damper's housing volume was measured to be $9,46 \times 10^5 \text{ mm}^3$, with the volume of each a component indicated as follows: piston with magnetic clamp and springs $3,2 \times 10^5 \text{ mm}^3$; magnets, $4,3 \times 10^5 \text{ mm}^3$; end plate, $6,3 \times 10^4 \text{ mm}^3$; damper cap $3,9 \times 10^4 \text{ mm}^3$; and damper body $9,4 \times 10^4 \text{ mm}^3$. The piston was connected to the damper body through a cylindrical contact to achieve friction-free performance, minimise frictional resistance, and ensure smooth operation. The fabricated damper, which incorporated the MPRD principle and springs, exhibited the desired behaviour and could effectively withstand the absorbed applied force. Figure 10 shows the prototype MPRD that visually represents the design.



Figure 10. Prototype model of the MPRD

4.4.2 Experimental setup for the testing of the magnetic pole repulsive damper

The primary purpose of the MPRD is to enhance the structural strength of joints during seismic events such as earthquakes. The MPRD was fixed to both sides of the joint to provide stability and support. Various loading patterns were applied to the MPRD and the resulting hysteretic graphs were carefully observed.

The performance of the MPRD was evaluated using a cyclic compression–tension force test. In the cyclic loading test, the MPRD was subjected to loading cycles to assess its ability to

withstand and dissipate energy during seismic events. The cyclic compression–tension test utilised a Material Testing System (MTS) 1000 kN universal testing machine (UTM) to simulate and observe the reaction of the MPRD.

Figure 11 shows the experimental setup for the MPRD test using the MTS UTM. Overall, these tests and observations helped evaluate the behaviour of the MPRD in improving the force and its ability to reduce the damaging effects of seismic activity.



Figure 11. Experimental setup of MPRD in the Material Testing System (MTS)

4.4.3 Cyclic behaviour of the magnetic pole repulsive damper

The MPRD consists of several parts, and the effect of the behaviour of the proposed MPRD was evaluated. Therefore, MPRDs with different displacements were experimentally tested and numerically simulated under cyclic loading. The positive direction refers to the spring's tension and the magnets' repulsive force, and the negative direction refers to the compression of the spring, which has the capacity of recentring.

Figure 12 displays the force–displacement hysteresis of the MPRD, showing both the experimental (black) and simulated (red) results obtained from the cyclic tensile-compressive tests. The maximum capacities of the cyclic force were determined through numerical simulation, resulting in $-2,877$, $-2,09$, $-1,226$, $-0,909$, and $-0,408$ kN in tension, and $2,877$; $1,960$; $1,231$; $0,912$ and $0,408$ kN in compression. Similarly, the experimental behaviour of the MPRD under cyclic loading was observed, with the maximum cyclic forces recorded as $-2,864$; $-2,081$; $-1,273$; $-0,926$ and $-0,4006$ kN in tension, and $2,870$; $2,242$; $1,226$; $0,926$ and $0,408$ kN in compression, respectively, for displacement rates of 5, 10, 15, 20, and 25 mm/min. A comparison of the simulated and experimental results showed a validation variation of 2,75 % for compression, whereas tension showed a negligible difference of 0,06 %.

The maximum strengths of the experimental results in the cyclic curves generally followed the same trend as those obtained from the numerical simulation, as confirmed by comparison. A comparison of the cyclic test results are tabulated in Table 9.

The cyclic test demonstrated the ability of the MPRD to exert forces at different displacements and showed the effective repulsive behaviour of the neodymium magnets during structural investigations without experiencing significant losses due to factors such as heat.

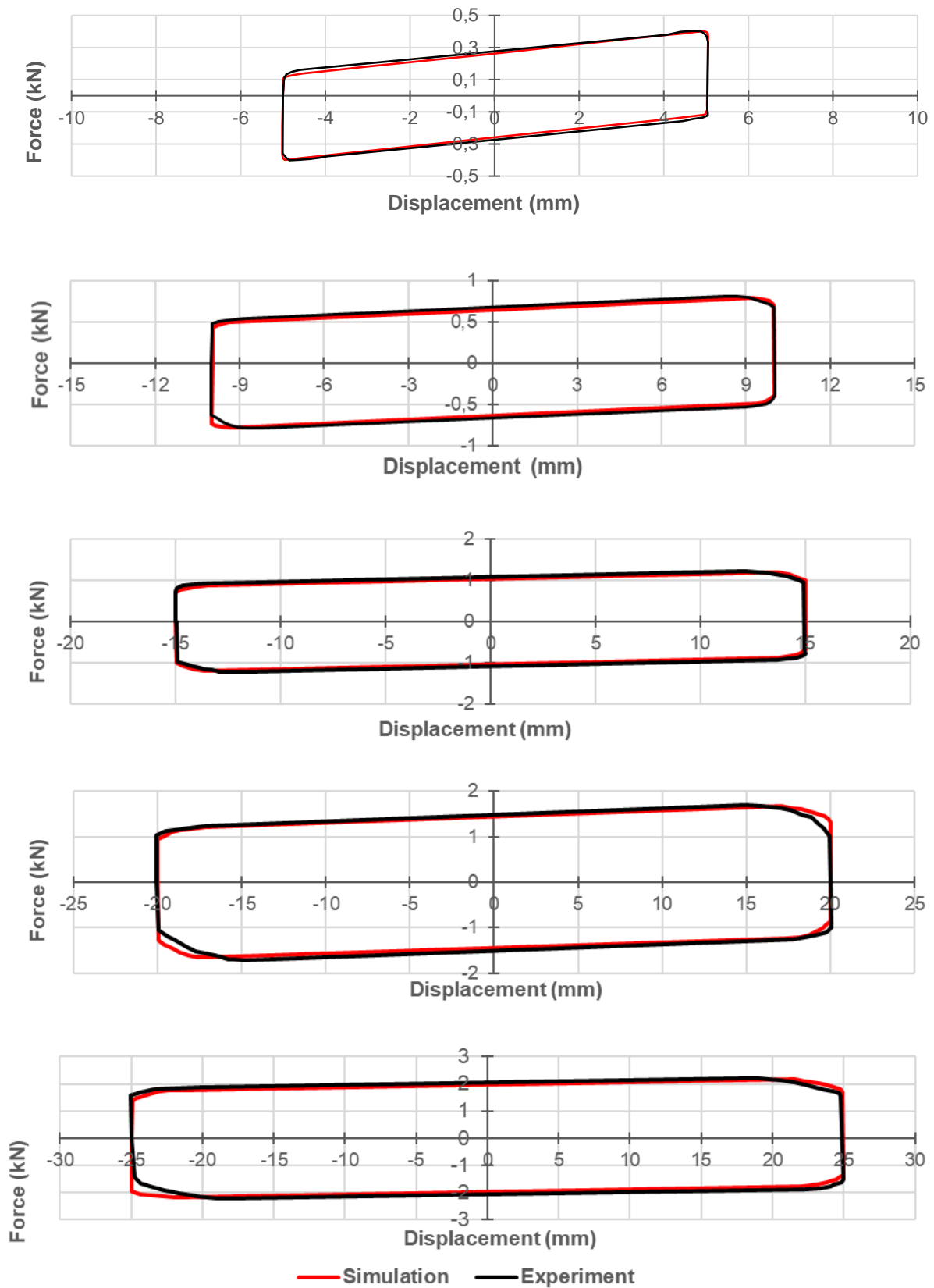


Figure 12. Comparison of numerical simulation and experimental test results of cyclic loading at 5, 10, 15, 20, and 25 mm.

Table 9. Comparison of experimental and simulation results

Displacement (mm)	Simulation results		Experimental results		Difference of experimental and simulated results (%)
	Maximum force in compression (kN)	Maximum force in tension (kN)	Maximum force in compression (kN)	Maximum force in tension (kN)	
5	0,408	-0,4006	0,408	-0,408	1,84
10	0,909	-0,9260	0,912	-0,930	0,43
15	1,226	-1,2730	1,231	-1,229	3,58
20	2,042	-2,0810	1,960	-2,090	0,48
25	2,800	-2,8640	2,877	-2,866	0,06

4.5 Results and discussion on the behaviour of the magnetic pole repulsive magnet

This investigation aimed to examine the behaviour of springs, magnets, and the MPRD, and the corresponding numerical simulations and experiments were performed. The maximum force-carrying capacity of the spring during the compression tests was 2,196 kN in the experiments and 2,2028 kN in the numerical simulations. Similarly, in the tension tests, it was -1,972 kN in the experiments and -1,962 kN in the numerical simulations. These results were analysed and the variation between the experiments and numerical simulations was 0,3% in compression and 0,5 % in tension, indicating good validation. The maximum capacity of the magnets was 1,3894 kN in the experimental tests and 1,465 kN in the numerical simulation at a displacement of 5 mm. The variation between the experimental and numerical values was 7,69 %. In the cyclic compression-tension tests of the MPRD, in the experiment, the forces were 2,877 kN (compression) and -2,866 kN (tension). Similarly, in the numerical simulation, the forces were 2,8 kN (compression) and -2,864 kN (tension). The validation variation was 2,75 % for compression and a negligible difference of 0,06 % for tension. The maximum strengths obtained from the experimental and numerical results followed similar trends, confirming the consistency between the two approaches.

5 Conclusions

This study comprehensively analysed the behaviour of the MPRD, which was validated through both the finite element analysis results obtained from the ANSYS model and experimental results. A numerically simulated model was used to conduct a parametric analysis and investigate the influence of the MPRD. Several key conclusions were drawn:

- The springs were subjected to numerical simulations and experimental testing, which revealed their ability to withstand a compressive force of 2,2028 kN in the simulation and 2,196 kN in the experiment. Similarly, the tensile force was -1,962 kN in the simulation and -1,972 kN in the experiment. The variations between the results of the experiment and numerical simulation were 0,3 % in compression and 0,5 % in tension, indicating good validation.
- Experimental testing and numerical simulations were conducted using a TTM to examine the repulsive force of the magnet. The experimental results showed a magnetic block force capacity of 1,3894 kN, whereas the numerical study indicated a force capacity of 1,465 kN. The variation between the experimental and numerical results was 7,69 %.
- In the cyclic compression-tension test, the experimental results of the MPRD showed that the maximum compressive force was 2,877 kN, whereas the maximum tensile force was -2,866 kN. In the numerical simulation, the maximum compressive force measured was 2,8 kN, whereas the maximum tensile force was -2,864 kN. By comparing the simulated and experimental results, the variation in the observed results was found to be 2,75 % for compression. A negligible difference of 0,06 % in tension was observed in the cyclic tensile-compressive test. The test indicated excellent

agreement between the physical behaviour of the MPRD and the numerical simulation. The results confirmed the accuracy and reliability of the MPRD.

Overall, this study successfully validated the behaviour of the MPRD through experimental and numerical simulations, demonstrating its effectiveness in controlling the forces. The MPRD exhibited promising performance and can be considered an effective solution for seismic resilience in areas with moderate to high seismicity. Therefore, the MPRD can be positioned diagonally to framed structures to improve joint stability. Incorporating the MPRD into structural joints reduces the risk of failure and reduces earthquake-induced damage. This integration improves the structural resilience and protects against catastrophic consequences. In future research, the MPRD can be modified to improve the stiffness of the magnets, the material properties of the spring can be modified, and the MPRD can be fixed diagonally in the RC beam-column joint to improve the strength of the joint.

Abbreviations

FEM - finite element method

MPRD - magnetic pole repulsive damper

TTM - tensile testing machine

T - tesla

NeFeb - neodymium magnets

N - north pole

S - south pole

MTS UTM - material testing system 1000 kN universal testing machine

MPa - megapascal

kN - kilonewton

mm - millimetre

sec - seconds

Acknowledgments

The author expresses their gratitude and acknowledges the support and facilities provided by the Structural Engineering Laboratory of the Department of Civil Engineering at Karunya Institute of Technology and Sciences. The authors appreciate the experimental facilities and setup made available to them during their research.

References

- [1] Soong, T. T.; Spencer Jr., B. F. Supplemental energy dissipation: state-of-the-art and state-of-the-practice. *Engineering Structures*, 2002, 24 (3), pp. 243-259. [https://doi.org/10.1016/S0141-0296\(01\)00092-X](https://doi.org/10.1016/S0141-0296(01)00092-X)
- [2] Gu, H. et al. Research on vibration mechanism and control technology of building structure under earthquake action. *Journal of Vibroengineering*, 2021, 23 (6), pp.1395-1406. <https://doi.org/10.21595/jve.2021.22090>
- [3] Soong, T. T.; Dargush, G. F. *Passive energy dissipation systems in structural engineering*. 1st edition, Wiley, 1997.
- [4] Symans, M. D. et al. Energy Dissipation Systems for Seismic Applications: Current Practice and Recent Developments. *Journal of Structural Engineering*, 2008, 134 (1), pp. 3-21. [https://doi.org/10.1061/\(ASCE\)0733-9445\(2008\)134:1\(3\)](https://doi.org/10.1061/(ASCE)0733-9445(2008)134:1(3))
- [5] Parulekar, Y. M.; Reddy, G. R. Passive response control systems for seismic response reduction: A state-of-the-art review. *International Journal of Structural Stability and Dynamics*, 2009, 09 (01), pp. 151-177. <https://doi.org/10.1142/S0219455409002965>
- [6] Aghlara, R.; Tahir, M. Md. A passive metallic damper with replaceable steel bar components for earthquake protection of structures. *Engineering Structures*, 2018, 159, pp. 185-197. <https://doi.org/10.1016/j.engstruct.2017.12.049>

- [7] Zahrai, S. M.; Mortezaigholi, M. H. Cyclic performance of an elliptical-shaped damper with shear diaphragms in chevron braced steel frames. *Journal of Earthquake Engineering*, 2018, 22 (7), pp. 1209-1232. <https://doi.org/10.1080/13632469.2016.1277436>
- [8] Li, H.-N.; Huang, Z.; Fu, X.; Li, G. A re-centering deformation-amplified shape memory alloy damper for mitigating seismic response of building structures. *Structural Control and Health Monitoring*, 2018, 25 (9). <https://doi.org/10.1002/stc.2233>
- [9] Dong, B.; Sause, R.; Ricles, J. M. Seismic Response and Performance of a Steel MRF Building with Nonlinear Viscous Dampers under DBE and MCE. *Journal of Structural Engineering*, 2016, 142 (6). [https://doi.org/10.1061/\(ASCE\)ST.1943-541X.0001482](https://doi.org/10.1061/(ASCE)ST.1943-541X.0001482)
- [10] Dong, B.; Sause, R.; Ricles, J. M. Seismic Response and Damage of Reduced-Strength Steel MRF Structures with Nonlinear Viscous Dampers. *Journal of Structural Engineering*, 2018, 144 (12). [https://doi.org/10.1061/\(ASCE\)ST.1943-541X.0002226](https://doi.org/10.1061/(ASCE)ST.1943-541X.0002226)
- [11] Dong, B.; Ricles, J. M. Simplified seismic design procedure for steel MRF structure with nonlinear viscous dampers. *Journal of Constructional Steel Research*, 2021, 185. <https://doi.org/10.1016/j.jcsr.2021.106857>
- [12] Cruze, D. et al. A Review on the Magnetorheological Fluid, Damper and Its Applications for Seismic Mitigation. *Civil Engineering Journal*, 2018, 4 (12), pp. 3058-3074. <https://doi.org/10.28991/cej-03091220>
- [13] Abebe, D. Y.; Kim, J. W.; Gwak, G.; Choi, J. H. Low-Cycled Hysteresis Characteristics of Circular Hollow Steel Damper Subjected to Inelastic Behaviour. *International Journal of Steel Structures*, 2019, 19, pp.157-167. <https://doi.org/10.1007/s13296-018-0097-8>
- [14] Koroğlu, M. A.; Köken, A.; Dere, Y. Use of different shaped steel slit dampers in beam to column connections of steel frames under cycling loading. *Advanced Steel Construction*, 2018, 14 (2), pp. 251-273.
- [15] Teruna, D. R.; Majid, T. A.; Budiono, B. Experimental Study of Hysteretic Steel Damper for Energy Dissipation Capacity. *Advances in Civil Engineering*, 2015, pp. 1-12. <https://doi.org/10.1155/2015/631726>
- [16] Shen, X.; Wang, X.; Ye, Q.; Ye, A. Seismic performance of Transverse Steel Damper seismic system for long span bridges. *Engineering Structures*, 2017, 141, pp. 14-28. <https://doi.org/10.1016/j.engstruct.2017.03.014>
- [17] Passenbrunner, J.; Jungmayr, G.; Amrhein, W. Design and analysis of a 1d actively stabilized system with viscoelastic damping support. *Actuators*, 2019, 8 (2). <https://doi.org/10.3390/act8020033>
- [18] Kashani, A.; Ramli, N. H. B. Compressive Visco-Elastic Damper as a Seismic Energy Dissipater in Diagonal Bracing Members. In: International Conference on Contemporary Iran on Civil Engineering Architecture and Urban Development. 16 August 2017, Teheran, Iran, 2017.
- [19] Sui, Y.; He, Z.; Xue, J.; Wu, Z. Experimental study and numerical analysis on seismic performance of steel beam-column damping joint in Chinese traditional style buildings. *The Structural Design of Tall and Special Buildings*, 2020, 29 (5). <https://doi.org/10.1002/tal.1710>
- [20] Mehrabi, M. H. et al. Modeling of a viscoelastic damper and its application in structural control. *PLoS ONE*, 2017, 12 (6). <https://doi.org/10.1371/journal.pone.0176480>
- [21] Kishiki, S. et al. Inspection of U-shaped steel dampers based on residual plastic deformation. *Engineering Structures*, 2021, 245. <https://doi.org/10.1016/j.engstruct.2021.112915>
- [22] Liu, W.; Guo, Y.; Dong, X.; He, W. Earthquake response control of a super high-rise structure subjected to long-period ground motions via a novel viscous damped system with multilever mechanism. *The Structural Design of Tall and Special Buildings*, 2019, 28 (7). <https://doi.org/10.1002/tal.1600>
- [23] Zhou, Y.; Li, H. Analysis of a high-rise steel structure with viscous damped outriggers. *The Structural Design of Tall and Special Buildings*, 2014, 23 (13), pp. 963-979. <https://doi.org/10.1002/tal.1098>

- [24] Skiedraitė, I. et al. Friction between steel plates under the influence of magnetic field. *Mechanika*, 2017, 23 (2), pp. 305-309. <https://doi.org/10.5755/j01.mech.23.2.13839>
- [25] Bissal, A.; Salinas, E.; Magnusson, J.; Engdahl, G. On the design of a linear composite magnetic damper. *IEEE Transactions on Magnetics*, 2015, 51 (11), pp. 1-5. <https://doi.org/10.1109/TMAG.2015.2440770>
- [26] Parlak, Z.; Engin, T.; Çallı, İ. Optimal design of MR damper via finite element analyses of fluid dynamic and magnetic field. *Mechatronics*, 2012, 22 (6), pp. 890-903. <https://doi.org/10.1016/j.mechatronics.2012.05.007>
- [27] Lahdo, M.; Ströhla, T.; Kovalev, S. Repulsive magnetic levitation force calculation for a high precision 6-DoF magnetic levitation positioning system. *IEEE Transactions on Magnetics*, 2017, 53 (3), pp. 1-6. <https://doi.org/10.1109/TMAG.2016.2636124>
- [28] Bekinal, S. I.; Deshwal, D.; Srinivas, V. G. Optimized multi-layer radial permanent magnet bearing with an eddy current damping systems. *Journal of the Brazilian Society of Mechanical Sciences and Engineering*, 2022, 44. <https://doi.org/10.1007/s40430-022-03855-7>
- [29] Wu, W.; Chen, X.; Shan, Y. Analysis and experiment of a vibration isolator using a novel magnetic spring with negative stiffness. *Journal of Sound and Vibration*, 2014, 333 (13), pp. 2958-2970. <https://doi.org/10.1016/j.jsv.2014.02.009>
- [30] Lavanya, N.; Rao, P. S.; Reddy, M. P. Design and analysis of a suspension coil spring for automotive vehicle. *International Journal of Engineering Research and Applications*, 2014, 4 (9), pp. 151-157.
- [31] Sreenivasan, M. et al. Finite element analysis of coil spring of a motorcycle suspension system using different fibre materials. *Materials Today: Proceedings*, 2020, 33 (1), pp. 275-279. <https://doi.org/10.1016/j.matpr.2020.04.051>
- [32] Zhu, Y. et al. Modelling and analysis of a negative stiffness magnetic suspension vibration isolator with experimental investigations. *Review of Scientific Instruments*, 2012, 83 (9). <https://doi.org/10.1063/1.4751863>
- [33] Choi, E.; Choi, G.; Kim, H. T.; Youn, H. Smart damper using the combination of magnetic friction and pre-compressed rubber springs. *Journal of Sound and Vibration*, 2015, 351, pp. 68-89. <https://doi.org/10.1016/j.jsv.2015.04.028>
- [34] Nims, D. K.; Richter, P. J.; Bachman, R. E. The use of the energy dissipating restraint for seismic hazard mitigation. *Earthquake Spectra*, 1993, 9 (3), pp. 467-489. <https://doi.org/10.1193/1.1585725>
- [35] Ozbulut, O. E.; Bitaraf, M.; Hurlebaus, S. Adaptive control of base-isolated structures against near-field earthquakes using variable friction dampers. *Engineering Structures*, 2011, 33 (12), pp. 3143-3154. <https://doi.org/10.1016/j.engstruct.2011.08.022>
- [36] Wasnik, P.; Sanghai, S.; Pawade, P. Y. Cyclic load Analysis of beam column joint using ANSYS. In: *IOP Conference Series: Materials Science and Engineering*, volume 1197. 25-26 June 2021, Guntur, India, IOP Science; 2021. <https://doi.org/10.1088/1757-899X/1197/1/012056>
- [37] Li, H.; Li, G. Earthquake-resistant design of RC frame with “dual functions” metallic dampers. In: *Proceedings of the ASME 2007 Pressure Vessels and Piping Conference. Volume 8: Seismic Engineering*. 22-26 July 2007, San Antonio, Texas, USA, ASME Digital Collection; 2007, pp. 43-53. <https://doi.org/10.1115/PVP2007-26450>
- [38] Wu, Z. et al. Dynamic experimental and numerical study of double beam–column joints in modern traditional-style steel buildings with viscous damper. *The Structural Design of Tall and Special Buildings*, 2020, 29 (1). <https://doi.org/10.1002/tal.1677>